



UNIVERSITY *of* York

This is a repository copy of *Endogenous driving and synchronization in cardiac and uterine virtual tissues: bifurcations and local coupling* .

White Rose Research Online URL for this paper:  
<http://eprints.whiterose.ac.uk/1310/>

---

**Article:**

Benson, A.P., Clayton, R.H., Holden, A.V. et al. (2 more authors) (2006) Endogenous driving and synchronization in cardiac and uterine virtual tissues: bifurcations and local coupling. *Philosophical Transactions of the Royal Society A: Mathematical, Physical and Engineering Sciences*, 364 (1842). pp. 1313-1327. ISSN 1471-2962

<https://doi.org/10.1098/rsta.2006.1772>

---

**Reuse**

See Attached

**Takedown**

If you consider content in White Rose Research Online to be in breach of UK law, please notify us by emailing [eprints@whiterose.ac.uk](mailto:eprints@whiterose.ac.uk) including the URL of the record and the reason for the withdrawal request.



[eprints@whiterose.ac.uk](mailto:eprints@whiterose.ac.uk)  
<https://eprints.whiterose.ac.uk/>

# Endogenous driving and synchronization in cardiac and uterine virtual tissues: bifurcations and local coupling

BY ALAN P. BENSON<sup>1</sup>, RICHARD H. CLAYTON<sup>2</sup>, ARUN V. HOLDEN<sup>1,\*</sup>,  
SANJAY KHARCHE<sup>1</sup> AND WING C. TONG<sup>1</sup>

<sup>1</sup>*Institute of Membrane and Systems Biology, and Cardiovascular Research  
Institute, University of Leeds, Leeds LS2 9JT, UK*

<sup>2</sup>*Department of Computer Science, University of Sheffield, Sheffield S1 4DP, UK*

Cardiac and uterine muscle cells and tissue can be either autorhythmic or excitable. These behaviours exchange stability at bifurcations produced by changes in parameters, which if spatially localized can produce an ectopic pacemaking focus. The effects of these parameters on cell dynamics have been identified and quantified using continuation algorithms and by numerical solutions of virtual cells. The ability of a compact pacemaker to drive the surrounding excitable tissues depends on both the size of the pacemaker and the strength of electrotonic coupling between cells within, between, and outside the pacemaking region.

We investigate an ectopic pacemaker surrounded by normal excitable tissue. Cell–cell coupling is simulated by the diffusion coefficient for voltage. For uniformly coupled tissues, the behaviour of the hybrid tissue can take one of the three forms: (i) the surrounding tissue electrotonically suppresses the pacemaker; (ii) depressed rate oscillatory activity in the pacemaker but no propagation; and (iii) pacemaker driving propagations into the excitable region.

However, real tissues are heterogeneous with spatial changes in cell–cell coupling. In the gravid uterus during early pregnancy, cells are weakly coupled, with the cell–cell coupling increasing during late pregnancy, allowing synchronous contractions during labour. These effects are investigated for a caricature uterine tissue by allowing both excitability and diffusion coefficient to vary stochastically with space, and for cardiac tissues by spatial gradients in the diffusion coefficient.

**Keywords:** pacemaking; ectopic focus; bifurcation; excitable medium

## 1. Introduction

An excitable cell has a stable resting potential, and only generates action potentials (APs) in response to an input or under abnormal conditions. Pacemaking cells are autorhythmic in the absence of an input and in physiological conditions, and can respond to inputs and changes in conditions by a change in the

\* Author for correspondence (a.v.holden@leeds.ac.uk).

One contribution of 13 to a Theme Issue ‘Biomathematical modelling I’.

rate or pattern of their periodicity. The qualitative differences between these two types of cell behaviours—excitability or autorhythmicity—result from the different parameters and kinetics of their excitation equations, all of which have the same form. Ionic current flow through the membrane charges or discharges the membrane capacitance, and for a unit area of cell membrane

$$C_m \frac{dV}{dt} = -I_{\text{ionic}}, \quad (1.1)$$

where  $C_m$  is the specific membrane capacitance,  $V$  is membrane potential and  $I_{\text{ionic}}$  the membrane current density, which is the sum of the current densities for the different ion-selective channels, pumps and exchangers. Differences in APs from different tissues, and different parts of the same tissue, result from differences in the expression of the different ion transport and sequestration proteins.

A bifurcation occurs in a dynamical system, such as equation (1.1), as the stability of a solution changes under variation of parameters, and is observable as a qualitative change in behaviour. The bifurcation is located at the parameter value at which a change in the stability of a solution occurs. An example is the emergence of periodic solutions at the point where an equilibrium solution loses its stability. For the Hodgkin–Huxley equations (Hodgkin & Huxley 1952), a subcritical Hopf bifurcation, into small amplitude, unstable periodic solutions, separates the stable resting excitable state from autorhythmicity, induced by an increase in extracellular calcium ( $\text{Ca}^{2+}$ ) concentration or a reduction in membrane maximal potassium ( $\text{K}^+$ ) conductance (Holden & Yoda 1981). These unstable solutions connect to large amplitude, stable periodic solutions that correspond to a periodic discharge of AP.

Cardiac sinoatrial pacemaker cells are autorhythmic (Zhang *et al.* 2000), while ventricular cells are excitable (Kleber & Rudy 2004), and normally require repetitive current flows from neighbouring excited cells to generate repetitive APs. However, under abnormal conditions, such as a reduction in the time-independent potassium current conductance  $g_{\text{K1}}$  (Miake *et al.* 2002, 2003) or intracellular sodium concentration ( $[\text{Na}^+]_i$ ) overload (Harrison *et al.* 1992), periodic activity can be induced in ventricular cells. The difference in behaviour between excitable and autorhythmic cells may be considered dynamically as a bifurcation occurring in parameter space, rather than mechanistically in terms of the ionic currents that contribute towards the pacemaker potential. In §3, we characterize the bifurcations into periodicity produced in virtual ventricular cells, brought about by: (i) block of the  $\text{Na}^+$ – $\text{K}^+$  pump current  $I_{\text{NaK}}$ , as seen during ischemia (Carmeliet 1999) and digitalis intoxication (Kass *et al.* 1978; Gheorghiadu *et al.* 2004) for example, and (ii) downregulation of the time-independent inward rectifying current  $I_{\text{K1}}$ , which helps to maintain the resting membrane potential in ventricular myocytes and suppresses autorhythmicity. Downregulation of  $I_{\text{K1}}$  has been proposed as a possible means of clinically inducing pacemaker activity in the ventricles by gene transfer, as an alternative to ventricular pacing by implanted electronic pacemaker (Miake *et al.* 2002). For autorhythmic activity in a compact cluster of pacemaking cells—such as the sinoatrial node or an ectopic focus—to drive surrounding tissues, the cluster needs to be large enough to generate sufficient current and appropriately coupled to the surrounding tissue. In §4, we examine effects of the width of a boundary zone between the autorhythmic and excitable tissues, and the coupling between

them. For gravid uterine muscle, there are changes in both the excitability of cells and the intercellular coupling between cells during late pregnancy. In §5, we examine these effects on the synchronization of electrical activity in simplified tissue models.

## 2. Numerical methods

### (a) Cardiac cells and tissues

The rate of change of  $V$  for a single ventricular myocyte is modelled using equation (1.1).  $I_{\text{ionic}}$  was provided by the Luo–Rudy dynamic model (LRd00; Luo & Rudy 1994) or by the human ventricular model (HVM) of ten Tusscher *et al.* (2004). Changes in ionic concentrations are also modelled:

$$\frac{d[B]}{dt} = \frac{-I_B \times A_{\text{cap}}}{\text{Vol}_C \times z_B \times F}, \quad (2.1)$$

where  $[B]$  is the concentration of ion B,  $I_B$  is the sum of the currents carrying ion B,  $A_{\text{cap}}$  is capacitive membrane area,  $\text{Vol}_C$  is the volume of the compartment whose concentration is being updated,  $z_B$  is the valence of ion B and  $F$  is Faraday's constant. Source codes written in C/C++ can be found at <http://www.cwru.edu/med/CBRTC/LRdOnline/LRdModel.htm> for LRd00, and at <http://www-binf.bio.uu.nl/khwjtuss/HVM> for HVM. For both models, we solved equations of the form (1.1) and (2.1) using a simple forward Euler method with a time-step of  $\Delta t=0.01$  ms.

The bifurcations between different qualitative types of behaviour of nonlinear dynamical systems can be studied in state space as one or more parameters in a dynamical system are varied smoothly. These can be mapped in parameter space by path-following or continuation algorithms that track bifurcations as lines in two-dimensional parameter space (Ermentrout 2002), e.g. AUTO86 (Doedel & Kernévez 1986; see <http://sourceforge.net/projects/auto2000/>). These packages reduce the identification, location and tracking of equilibrium and periodic solution branches and other bifurcation problems to the continuation of implicitly defined curves, using predictor–corrector methods. For simplicity, consider autonomous dynamical systems and one-parameter bifurcation diagrams that contain equilibria, periodic solutions and Hopf and homoclinic bifurcations. Once a point on a particular branch is located, a continuation package follows the locus of either equilibrium or periodic states on the branch. While following an equilibrium branch, tracking the real parts (and signs) of the eigenvalues gives the stability of the branch that is exchanged between stable and unstable as the real part passes through zero. If a single complex conjugate pair of eigenvalues crosses the imaginary axis, small amplitude (stable or unstable) oscillations emerge at a Hopf bifurcation. Once the bifurcation point is found, continuation can be switched from the equilibrium to the periodic branch. The stability of periodic oscillations is followed using Floquet multipliers.

An autonomous dynamical system with one parameter of interest may be written as

$$\frac{d\mathbf{x}}{dt} = f(\mathbf{x}, \mu), \quad (2.2)$$

where  $\mathbf{x}$  is an  $n$ -dimensional vector of real numbers, and  $\mu$  is a parameter.  $\mathbf{x}$  may denote the vector of variables in the system of ordinary differential equations (ODEs) defining a cardiac cell model.  $\mu$  is the parameter whose variation causes a qualitative change in the behaviour of the model, such as a membrane maximal conductance. Equilibria are found from the solution of

$$f(\mathbf{x}_0, \mu_0) = 0. \quad (2.3)$$

The Jacobian of the above vector is defined as an  $n \times n$  matrix,  $\mathbf{J} = \partial f / \partial \mathbf{x} |_{\mathbf{x}_0}$ . If all the eigenvalues of  $\mathbf{J}$  have negative real parts, then the steady state is stable. If an eigenvalue has a positive real part, then the steady state is unstable, at least along a sub-manifold. If the equilibrium is a saddle point (i.e. eigenvalues with positive and negative real parts coexist), and the stable and unstable manifolds overlap, then it is associated with homoclinic orbits. Such orbits start and end at the saddle point and are characterized by infinite periods. While computing these orbits, we have to follow the periodic branches emerging from Hopf bifurcation points in one-parameter bifurcation diagrams. Homoclinic bifurcations occur when homoclinic orbits separate phase space regions of periodic orbits and non-periodic orbits. Although homoclinic bifurcations are global and cannot be detected by local continuation, they can be studied numerically by the methods given in [Champneys \*et al.\* \(1996\)](#).

Since excitation equations are constructed from a series of voltage and patch clamp experiments under different conditions, although they may successfully reproduce APs, they need not be electrochemically neutral, and so may not have physiologically meaningful equilibrium solutions. Further, they may not be posed in the form of dynamical systems: for example, in LRd00 the intracellular  $\text{Ca}^{2+}$  is triggered a delay after the peak of the AP. Continuation algorithms may only be applicable to reduced parts of the full excitation system, and so may have to be combined with numerical integration of the full system.

For studying propagation in cardiac tissues, we model one-dimensional tissue strands using the equation

$$\frac{\partial V}{\partial t} = \nabla(D\nabla V) - I_{\text{ionic}}, \quad (2.4)$$

where  $\nabla$  is a spatial gradient operator and  $D$  a diffusion coefficient. No-flux boundary conditions were imposed at the ends of the strands. A time-step of  $\Delta t = 0.02$  ms and a space step of  $\Delta x = 0.2$  mm were used in one-dimensional simulations.

#### (b) Uterine tissue

We simulate excitation in two-dimensional uterine tissue using a modified form of the FitzHugh–Nagumo model ([FitzHugh 1961](#); [Nagumo \*et al.\* 1962](#)):

$$\frac{\partial u}{\partial t} = \nabla D(x, y) \nabla u + ku(u - u_a)(u - 1) - v - I(x, y), \quad (2.5)$$

$$\frac{\partial v}{\partial t} = \epsilon(Gu - v), \quad (2.6)$$

where  $u$  is the excitation variable,  $v$  is the recovery variable,  $I$  is an input current controlling excitation,  $x$  and  $y$  denote space, and the constants  $k=8$ ,  $u_a=0.1$ ,

$\epsilon=0.02$  and  $G=5$  are membrane kinetic parameters. Behaviour of the tissue was examined as  $I$  and  $D$  were varied over the range 0–0.5. The two-dimensional tissue was simulated as a  $300 \times 400$  node Cartesian grid with a space step of  $\Delta x = \Delta y = 0.4$  space units, and was solved using a simple forward Euler step method with a time-step of  $\Delta t = 0.01$  time units.

### 3. Bifurcations in ventricular cells

#### (a) $I_{\text{NaK}}$ block and intracellular $\text{Ca}^{2+}$ oscillations

Block of  $I_{\text{NaK}}$  was examined in the endocardial LRd00 model. Kass *et al.* (1978) proposed that  $I_{\text{NaK}}$  block can induce ectopic pacemaking activity by increasing  $[\text{Na}^+]_i$  which in turn causes  $[\text{Ca}^{2+}]_i$  overload through the action of the  $\text{Na}^+ - \text{Ca}^{2+}$  exchanger. This can result in  $[\text{Ca}^{2+}]_i$  oscillations as  $\text{Ca}^{2+}$  is spontaneously released from, and is subsequently sequestered back into, the sarcoplasmic reticulum. These  $[\text{Ca}^{2+}]_i$  oscillations can interact with membrane currents, which in turn affect  $V$  and induce pacemaker activity. As the use of continuation algorithms is not feasible for LRd00 (§2a), numerical solutions were obtained in order to identify bifurcations that lead to autorhythmicity. We examined the emergence of  $[\text{Ca}^{2+}]_i$  oscillations during  $I_{\text{NaK}}$  block and the subsequent  $[\text{Na}^+]_i$  overload by clamping  $V$  and all  $\text{Na}^+$  and  $\text{K}^+$  concentrations, and so reducing the full LRd00 system to those equations describing  $\text{Ca}^{2+}$  handling. Behaviour of the  $\text{Ca}^{2+}$  handling equations was determined by numerical integration over a period of 120 s, where  $[\text{Ca}^{2+}]_i$  either settled to a stationary stable state or oscillated. With  $V$  clamped at  $-90$  mV and as the primary bifurcation parameter  $[\text{Na}^+]_i$  is increased to approximately 16.1 mM, large period  $[\text{Ca}^{2+}]_i$  oscillations emerge (figure 1a). The period of the oscillations decreases rapidly as  $[\text{Na}^+]_i$  is further increased (figure 1b), indicative of a homoclinic bifurcation rather than the Hopf bifurcation identified by Varghese & Winslow (1993) in the calcium subsystem of the DiFrancesco–Noble Purkinje fibre model (DiFrancesco & Noble 1985). Changes to the amplitude and period of the  $[\text{Ca}^{2+}]_i$  oscillations also occur with changes in the secondary bifurcation parameter  $V$  (figure 1c). With an increase in clamped  $V$  from  $-90$  to  $-70$  mV (and with  $[\text{Na}^+]_i$  clamped at 20 mM), increases in diastolic and systolic  $[\text{Ca}^{2+}]_i$  are observed along with a decrease in the period of the oscillations. The effects of changing both the primary and secondary bifurcation parameters on the  $[\text{Ca}^{2+}]_i$  subsystem dynamics are shown in figure 1d.

In the LRd00 cell model with  $I_{\text{ns(Ca)}}$  and  $I_{\text{K(Na)}}$  included, and parameters modified to induce  $[\text{Ca}^{2+}]_i$  oscillations—constant  $[\text{K}^+]_i = (310 - 3[\text{Na}^+]_i)/2$  mM (Varghese & Winslow 1994),  $I_{\text{NaK}}$  block,  $P_{\text{ns(Ca)}} = 3.5 \times 10^{-7}$  cm s $^{-1}$ ,  $[\text{CSQN}]_{\text{th}} = 7.0$  mM and the time constants of activation and inactivation of  $I_{\text{rel,jsrol}}$  increased to 5 ms—the oscillations seen in the  $\text{Ca}^{2+}$  handling system interact with the  $\text{Na}^+ - \text{Ca}^{2+}$  exchanger current  $I_{\text{NaCa}}$  and the non-specific  $\text{Ca}^{2+}$ -activated current  $I_{\text{ns(Ca)}}$  to cause pacemaker activity. With  $[\text{Na}^+]_i$  set to 20 mM, autorhythmic APs seen during the first 20 s of integration (figure 2a) become stable  $V$  oscillations between  $-13$  and  $-21$  mV. The corresponding  $[\text{Ca}^{2+}]_i$  oscillations (figure 2b) that drive these  $V$  oscillations take approximately 40 s to become stable. This transient behaviour is shown in the phase portraits of figure 2c,d; figure 2c shows

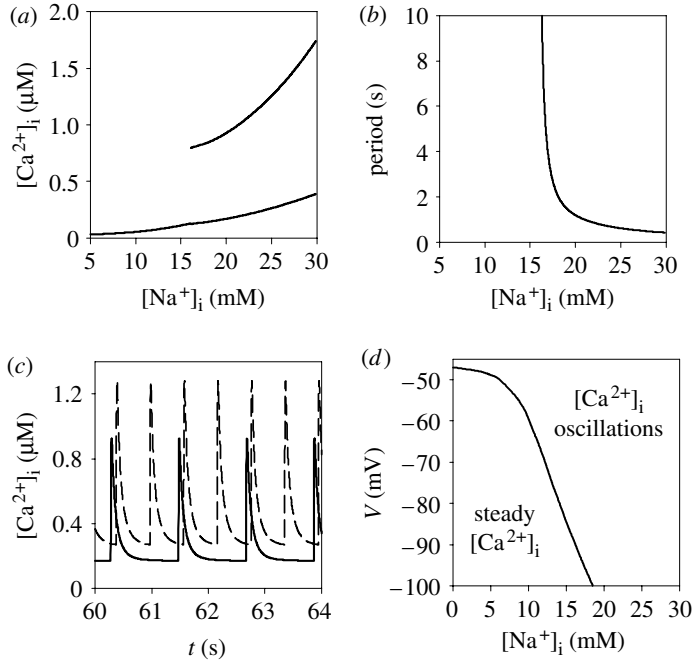


Figure 1. Numerical bifurcation analysis of the reduced LRd00 Ca<sup>2+</sup> system. (a) One-parameter bifurcation diagram with  $V$  clamped at  $-90$  mV. At low levels of  $[\text{Na}^+]_i$ ,  $[\text{Ca}^{2+}]_i$  settles to a steady state; as  $[\text{Na}^+]_i$  is increased to approximately 16.1 mM, oscillations emerge. (b) The corresponding periods of the oscillations shown in panel (a), truncated at 10 s. As  $[\text{Na}^+]_i$  is reduced towards the bifurcation, the period increases to unreasonably long values (greater than 80 s in our numerical integrations). (c) Effects of changing the secondary bifurcation parameter of the reduced system,  $V$ , on the  $[\text{Ca}^{2+}]_i$  oscillations. Solid line shows oscillations at  $V = -90$  mV, dashed line shows oscillations at  $V = -70$  mV. The increase in  $V$  results in increased diastolic and systolic  $[\text{Ca}^{2+}]_i$ , a larger oscillation amplitude and a reduced period. (d) Two-parameter bifurcation diagram showing  $[\text{Ca}^{2+}]_i$  steady states and oscillations in  $[\text{Na}^+]_i$ - $V$  parameter space.

the full 120 s of integration including the transient behaviour, figure 2d shows the period 60–120 s, when  $V$  and  $[\text{Ca}^{2+}]_i$  oscillations have become stable.

### (b) $I_{K1}$ downregulation

Both LRd00 and the epicardial HVM were used to identify bifurcations and autorhythmicity due to downregulation of  $I_{K1}$ . Clinically, mutations in a subunit of the  $I_{K1}$  channel are implicated in long QT syndrome 7, which has been associated with a loss of function (Tristani-Firouzi *et al.* 2002), and experimentally, downregulation of  $I_{K1}$  has been shown to induce autorhythmicity in ventricular cells (Miake *et al.* 2002, 2003). Downregulation of  $I_{K1}$  was modelled by multiplying  $g_{K1}$  by a fractional term  $x$ , where  $0 \leq x < 1$  represents downregulation.

In both systems, autorhythmic APs were seen when  $I_{K1}$  was completely blocked (fractional  $g_{K1} = 0$ ); the membrane potential remained stable when  $I_{K1}$  was not suppressed (fractional  $g_{K1} = 1$ ). Between these two extremes, a bifurcation occurred. In LRd00 (figure 3a), the bifurcation points of different ventricular cell types, although different, are very close (fractional  $g_{K1} \approx 0.3$ ).

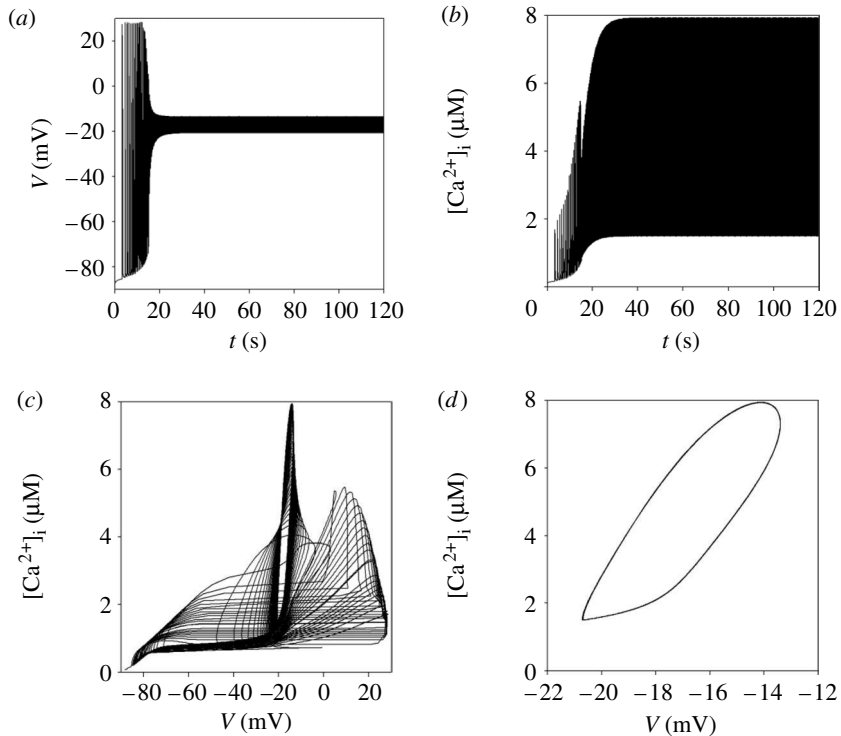


Figure 2. Time-series showing  $V$  (a) and  $[\text{Ca}^{2+}]_i$  (b) for a modified LRd00 myocyte (see §3a) integrated for 120 s with no stimulation. Panels (c) and (d) show phase portraits with  $[\text{Ca}^{2+}]_i$  plotted against  $V$  for the whole 120 s (c) and for the period 60–120 s (d).

However, for a given value of fractional  $g_{\text{K1}}$  below the bifurcation point, oscillations in M cells have the fastest rate, followed by endocardial then epicardial cells; channel densities determine the location of the bifurcation in parameter space as well as the rate of the oscillating system. As they have the fastest rate, any M cells within an ectopic focus will drive the pacemaking. HVM showed similar behaviour but with smaller bifurcation values in both the full system (figure 3b, fractional  $g_{\text{K1}} \approx 0.077$ ) and a reduced system with no ionic concentration dynamics (figure 3c, fractional  $g_{\text{K1}} \approx 0.05$ ). The different bifurcation values of the two HVM systems shows that, in addition to channel densities, ionic concentrations play a part in determining the location of the bifurcation and the emergent behaviour. For downregulation to be an effective therapy, a ‘reasonable’ downregulation needs to be effective: comparing these results to guinea-pig experiments (Miake *et al.* 2002, 2003) and computational models (Silva & Rudy 2003), a greater reduction of  $I_{\text{K1}}$  is required for pacemaker activity to be induced in human ventricular cells.

All systems showed a rapid decrease in the period of the oscillations immediately after the bifurcation. This numerical evidence suggests homoclinic bifurcations. If pacemaking is to be induced by progressively developing downregulation of  $g_{\text{K1}}$ , the induced pacemaker would start with an unreasonably long period; this would be suppressed by the electrical driving of the residual normal pacemaking and is potentially arrhythmogenic.

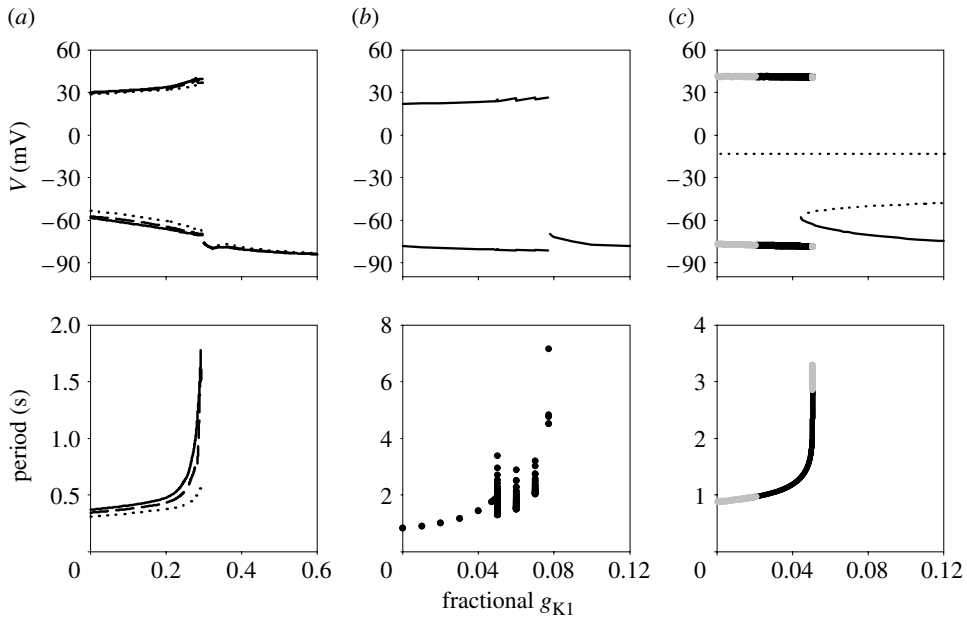


Figure 3. Bifurcation analysis on two different mammalian ventricular cell models. (a) LRd00 (solid line—epicardial; dotted line—M cells; dashed line—endocardial) and (b) the full HVM system. Both systems are solved numerically. (c) A reduced system of HVM without ionic concentration dynamics, with the bifurcation computed using XPPAUT (Ermentrout 2002). Black and solid lines—stable solutions, grey and dotted lines—unstable solutions. The upper panels show  $V$  when the bifurcation parameter  $g_{K1}$  is changed by a fractional term. The lower panels show the corresponding oscillation periods. In addition, multiple periods are observed in the full, numerically solved HVM system, where bursts of oscillations following a parabolic rhythm are interrupted by periods of quiescent states. This phenomenon is further discussed in Benson *et al.* (2005) and Tong & Holden (2005).

#### 4. Pacemaker driving of surrounding tissue

##### (a) Effects of a border zone between pacemaking and excitable tissues

The effects of pacemaker size on the ability of that pacemaker to drive surrounding tissue have been examined for various cardiac tissues (e.g. Fozzard & Schoenberg 1972; Lindemans & Vandergon 1978; Winslow *et al.* 1993; Joyner *et al.* 2000; Wilders *et al.* 2000; Carey *et al.* 2001). These studies assumed that the border between the two tissues was distinct, and that parameter values inducing autorhythmicity changed in a stepwise fashion between the two tissues. We include a border zone between the pacemaking tissue and the normal excitable tissue by adding an area between the two tissues where parameter values and initial conditions change smoothly in space. Using block of  $I_{NaK}$  to induce pacemaking (§3a) located at one end of a 15 mm LRd00 endocardial one-dimensional strand, the parameters are changed either linearly or sigmoidally between the two tissues. For sigmoidal changes, parameters are scaled by  $f(x) = 1/(1 + e^{-ax})$ , where  $a$  is a constant and  $x$  denotes space within the border zone. Figure 4 shows the effects of these different spatial changes of parameter

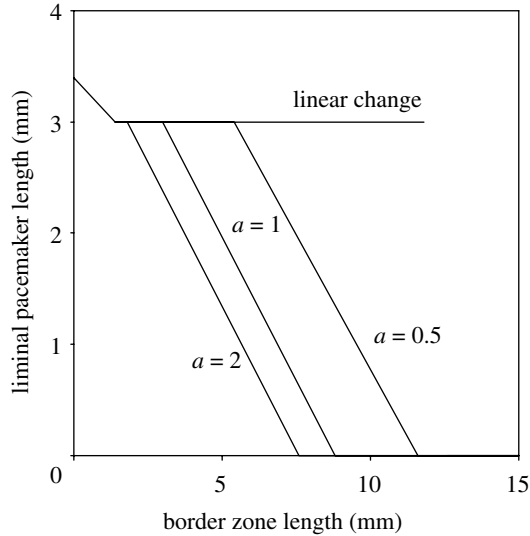


Figure 4. Liminal length of pacemaker tissue required to produce propagation of an action potential along a 15 mm endocardial LRd00 strand with homogeneous  $D=0.06 \text{ mm}^2 \text{ ms}^{-1}$ , as a function of the size of border zone between the pacemaking and excitable tissue. Parameter value changes in the border zone occur between the values of the pacemaker and excitable tissues either linearly or sigmoidally; in all cases, the absolute change in parameter values is the same. With linear changes in a border zone greater than 12 mm, the tissue length is not large enough to accommodate the required liminal length and so propagation fails. For sigmoidal changes, and with border zone lengths greater than 7.6, 9.0 and 11.6 mm for  $a=2$ , 1 and 0.5, respectively, the border zone itself can act as a pacemaker and so no central pacemaking tissue is required for propagation.

values within the border zone on the liminal length of pacemaker tissue required to drive propagation. In all cases, the absolute changes in parameter values between the pacemaking and excitable tissues are the same: only the spatial rate of change of parameter values in the border zone varies. When the spatial change is linear, liminal pacemaker length decreases from 3.4 to 3.0 mm as the border zone is increased in size from 0 to 3.0 mm. Further increases in border zone size do not cause a further reduction in liminal pacemaker length. With sigmoidal changes of parameter values within the border zone where  $a=0.5$ , 1 or 2, the liminal pacemaker length is gradually decreased as border zone length increases. When the border zone length is larger than 11.6, 9.0 and 7.6 mm for  $a=0.5$ , 1 and 2, respectively, the border zone itself can act as a pacemaker and so no central pacemaker tissue is required for propagation. The differences between the effects of linear and the different sigmoidal changes within the border zone suggest that the rate of change of the parameter values with respect to space is more relevant than the absolute change in parameter value. When the spatial rate of change of parameter values in the border zone near the pacemaking tissue is low (e.g. with a sigmoidal change where  $a=2$ ), more border zone tissue is raised above the threshold at which it becomes autorhythmic. If the rate of change is high (e.g. with a linear change), less border zone tissue is above the autorhythmic threshold, therefore increasing the length of pacemaker tissue required to drive propagation.

(b) *Effects of spatial changes in the diffusion coefficient*

Propagation through excitable media, such as cardiac and uterine muscle, depends on the diffusion coefficient,  $D$ , that is used to model current flow through intercellular gap junctions. The examples of propagation along a one-dimensional strand presented in §4a have all been in uniformly coupled tissues, i.e.  $D$  is spatially homogeneous. However, the coupling in real tissues is heterogeneous, e.g. cell–cell uncoupling during ischemia (Carmeliet 1999) or transmural differences (Yan *et al.* 1998; Gima & Rudy 2002). We altered intercellular coupling by changing  $D$  within pacemaking tissue and within a border zone separating the pacemaker from the excitable tissue. Figure 5a shows the effects of changing the length of the pacemaking tissue (tissue with  $I_{\text{NaK}}$  block, §3a) and the diffusion coefficient within the pacemaker,  $D_{\text{P}}$ , located at one end of a 15 mm endocardial LRd00 strand with no border zone. Three types of behaviour are observed. At low pacemaker lengths, the electrotonic influence of the excitable tissue suppresses the pacemaker activity, resulting in sub-threshold  $V$  oscillations within the pacemaking tissue. For values of  $D_{\text{P}}$  approximately larger than  $0.018 \text{ mm}^2 \text{ ms}^{-1}$  and for pacemaker lengths larger than the liminal length for that particular tissue, the voltage oscillations in the pacemaker tissue reach threshold, resulting in APs that propagate into the excitable tissue and along the strand. For values of  $D_{\text{P}}$  approximately smaller than  $0.018 \text{ mm}^2 \text{ ms}^{-1}$ , however, propagation is not achieved. The electrotonic influence of neighbouring tissues is minimal and the tissue behaves as a series of uncoupled individual cells rather than a functional syncytium. Here, there are APs within the pacemaker but, due to the low coupling, no propagation into the excitable tissue. These three types of behaviour are illustrated in the space–time plots of figure 5b–d. Figure 5b shows a pacemaking tissue of length 2 mm with  $D_{\text{P}} = 0.05 \text{ mm}^2 \text{ ms}^{-1}$  in which pacemaker activity is suppressed. In figure 5c, the pacemaker length (4 mm) is supra-liminal for the diffusion coefficient  $D_{\text{P}} = 0.05 \text{ mm}^2 \text{ ms}^{-1}$  and so propagation occurs along the strand. In figure 5d,  $D_{\text{P}}$  is reduced to  $0.01 \text{ mm}^2 \text{ ms}^{-1}$  with the pacemaker length at 4 mm: periodic APs are observed in the pacemaker but they do not propagate into the excitable tissue. Qualitatively similar results are found when either a linearly changing or sigmoidally changing ( $a=1$ ) 2 mm border zone is introduced between the pacemaker and excitable tissues (results not shown). Similar behaviour was observed by Wilders *et al.* (2000) in a two-dimensional sheet of ventricular cells where a single sinoatrial node model acted as the pacemaker, with the coupling currents associated with this node scaled in order to simulate variations in the size of the pacemaker.

## 5. Synchronization and bursting

During early pregnancy, local contractions of the uterine muscle occur, and as pregnancy progresses, the amplitude of contractions increases (Wray 1993). In advanced pregnancy, the contractions involve most of the uterine tissue. There is an increase in activity and in synchronization of activity during late pregnancy: the increase in synchronization correlates with an increase in the density of gap junctions (Garfield *et al.* 1995). In terms of dynamics, there is an increase in activity, from a predominantly resting to a predominantly periodic state, and an

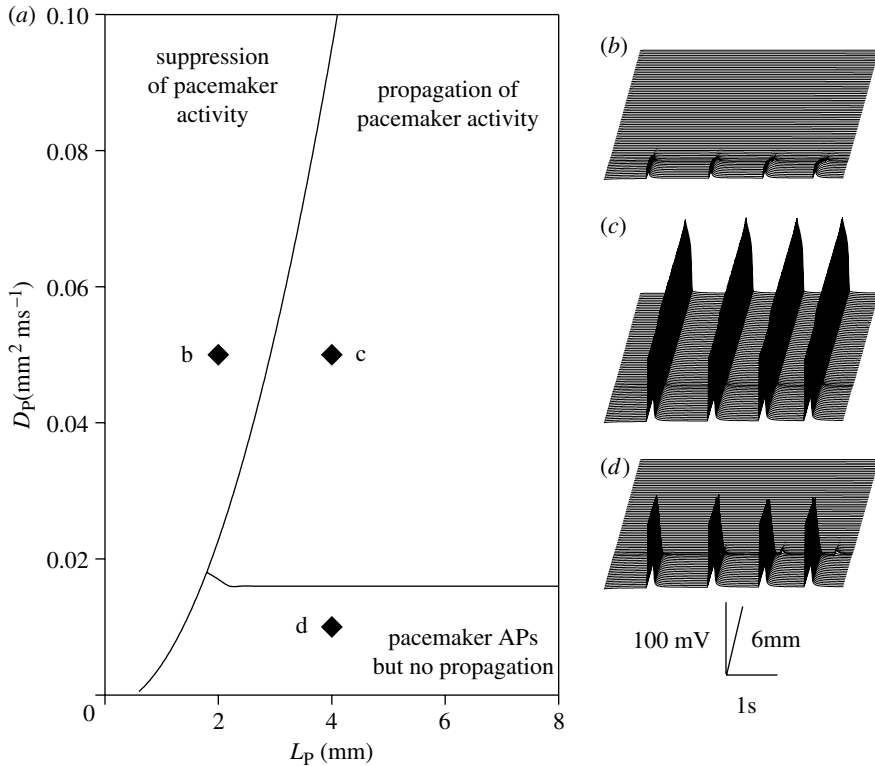


Figure 5. (a) Behaviour of pacemaking activity in a 15 mm endocardial LRd00 strand with modified pacemaker tissue located at one end (no border zone), as the pacemaker length ( $L_P$ ) and the diffusion coefficient within the pacemaker ( $D_P$ ) are changed. The diffusion coefficient in the excitable tissue is constant at  $0.06 \text{ mm}^2 \text{ ms}^{-1}$ . Behaviour can take one of the three forms, as shown in the space–time plots of panels (b–d). (b) With  $D_P=0.05 \text{ mm}^2 \text{ ms}^{-1}$  and a sub-liminal  $L_P$  of 2 mm, electrotonic currents suppress the pacemaker activity, resulting in sub-threshold  $V$  oscillations. (c) When  $D_P$  is the same ( $0.05 \text{ mm}^2 \text{ ms}^{-1}$ ) but  $L_P$  is increased to 4 mm (supra-liminal), oscillatory action potentials in the pacemaking tissue propagate into the excitable tissue and along the strand. (d) As cells are uncoupled and  $D_P$  falls to  $0.01 \text{ mm}^2 \text{ ms}^{-1}$  ( $L_P$  remaining at 4 mm), action potentials are observed in the pacemaking tissue but propagation fails. The locations of panels (b–d) in  $D_P$ – $L_P$  parameter space are indicated in panel (a).

increase in coupling. We caricature these patterns of activity by a two-dimensional excitable medium, in which activity and coupling were distributed randomly with FitzHugh–Nagumo kinetics (equations (2.5) and (2.6)). As there are no anatomically defined pacemaker sites in the uterus, we allowed the two parameters  $I$  and  $D$  to vary randomly throughout the medium. At each gridpoint in the medium,  $I$  and  $D$  had a fixed value, selected from a Gaussian distribution around a given mean  $\langle I \rangle$ ,  $\langle D \rangle$  in the range from 0 to 0.5, with standard deviation of 0.15. The parameter  $I$  is a bifurcation parameter for the FitzHugh–Nagumo ordinary differential system, and for our parameter set a Hopf bifurcation into periodic, AP-like oscillations occurs at  $I$  close to 0.25. The equilibrium solution regains its stability at  $I$  close to 2.2, and so, within the range used, the parameter  $I$  specifies whether a node is excitable or autorhythmic and, if autorhythmic, its rate. The diffusion coefficient  $D$  was used to simulate the cell–cell coupling.

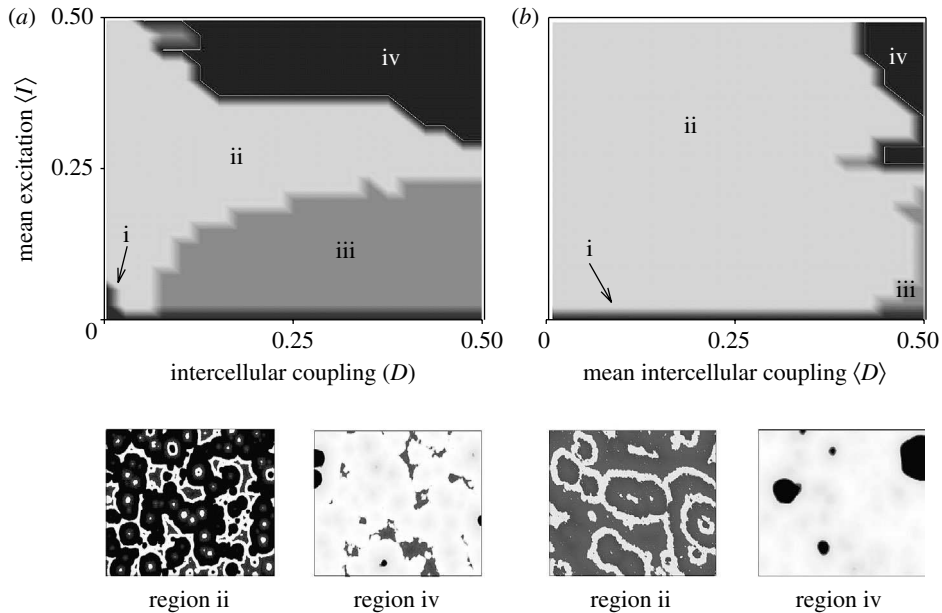


Figure 6. Effects of excitation and coupling on synchronization behaviour in two-dimensional FitzHugh–Nagumo excitable medium caricaturing uterine muscle. Behaviours are mapped into the parameter space of the mean value of the bifurcation parameter,  $\langle I \rangle$ , and the diffusion coefficient  $D$  (a) or its mean  $\langle D \rangle$  (b). In panel (a),  $I$  is randomly distributed in space, while  $D$  is constant; in panel (b), both  $I$  and  $D$  are randomly distributed in space. The four behaviours (i)–(iv) described in §5 and identified from movies of simulations are colour coded, and example frames of the distribution of the excitation variable  $V$  are shown in the bottom panels: light is excited and dark is resting.

The qualitative behaviour of the system is presented in parameter space of  $\langle I \rangle$  and  $\langle D \rangle$ , where qualitatively different regions were identified, as illustrated in figure 6. We constructed the parameter space with either only  $I$  or  $D$ , and with both  $I$  and  $D$  randomly distributed over the two-dimensional model. Four types of behaviour were classified from space–time movies:

- (i) Activity is spatially sparse, leading to a low level of spatially integrated activity. At any one active node, the size of the AP is reduced, as a result of electrotonic spread to surrounding tissue.
- (ii) Spatial clustered activity, each cluster acting as a localized focus emitting periodic waves. Activity at any one node is burst-like, alternating between different rates of repetitive APs, or between repetitive activity and silence.
- (iii) Moderate level of almost spatially uniform excitation: at any one node there is a maintained depolarization, or small amplitude oscillations around a maintained depolarization.
- (iv) Predominantly spatially coherent synchronous discharge of APs.

For low values of parameters  $\langle I \rangle$  and  $D$  or  $\langle D \rangle$ , activity was spatially localized and asynchronous. As the value of  $\langle I \rangle$  was increased, the activity increased, in frequency and integrated amplitude. With an increase in the value of  $D$  or  $\langle D \rangle$ , there was an increase in spatial coherence, i.e. larger space scales and temporal synchronization of activity was observed.

## 6. Conclusions

The differences between normal pacemaking and excitable cells can be understood in terms of the stability of their equilibrium states: an excitable tissue, such as normal ventricular cells, has a stable resting potential that corresponds to a stable equilibrium, while a pacemaking cell has a stable periodic state. These states are separated in parameter space by bifurcations. For ODE models of the electrical activity of single cells, if they are electrochemically neutral with physiologically sensible equilibrium states, bifurcations can be mapped in parameter space using continuation algorithms. If the cell model is not electrochemically neutral, and so does not have a stable resting state, or if the cell model is not formulated as a differential system, bifurcations can still be mapped by a combination of numerical integrations and the application of continuation algorithms to reduced systems.

Automaticity can be induced in ventricular cell models, by reducing a repolarizing conductance, or by blocking an ion-exchange process. In both cases, automaticity is produced by a homoclinic bifurcation—the emergence of very long-period oscillations—rather than by a Hopf bifurcation. If such automaticity is to act as an ectopic pacemaker, driving the surrounding tissue, the effectiveness and minimal size of the pacemaking tissue depends on the coupling within and between the pacemaker and the excitable tissue.

In virtual uterine tissue, spatial heterogeneity is seen to assist transitions between quiescence, bursting, synchrony and quenched systems. A spatial heterogeneity in intercellular coupling on its own does not permit large-scale synchronous behaviour within the parameter range investigated. Simultaneous heterogeneity in excitation and intercellular coupling, however, increases the possibility of bursting.

## Editors' note

Please see also related communications in this focussed issue by [Biktasheva \*et al.\* \(2006\)](#) and [Fink \*et al.\* \(2006\)](#).

This work is supported by grants from the MRC (G0000315), the EPSRC (GR/S43498/01, GR/R92592/01, GR/R40838/01) and the EU Network of Excellence 'BioSim' (005137). A.P.B. is supported by an MRC bio-informatics (computational biology) priority area research studentship (G74/63), W.C.T. by a BHF research studentship (FS/03/075/15914).

## References

- Benson, A. P., Holden, A. V., Kharche, S. & Tong, W. C. 2005 From gene expression to tissue dynamics, via continuation algorithms: ectopic pacemaking in the heart. In *Proc. Int. Workshop on Computational Methods in Systems Biology, Edinburgh, UK, 3–5 April 2005*, pp. 192–203.
- Biktasheva, I. V., Simitev, R. D., Suckley, R. & Biktashev, V. N. 2006 Asymptotic properties of mathematical models of excitability. *Phil. Trans. R. Soc. A* **364**, 1283–1298. (doi:10.1098/rsta.2006.1770)
- Carey, P. A., Turner, M., Fry, C. H. & Sheridan, D. J. 2001 Reduced anisotropy of action potential conduction in left ventricular hypertrophy. *J. Cardiovasc. Electrophysiol.* **12**, 830–835. (doi:10.1046/j.1540-8167.2001.00830.x)

- Carmeliet, E. 1999 Cardiac ionic currents and acute ischemia: from channels to arrhythmias. *Physiol. Rev.* **79**, 917–1017.
- Champneys, A. R., Kuznetsov, Y. A. & Sandstede, B. 1996 A numerical toolbox for homoclinic bifurcation analysis. *Int. J. Bifurcat. Chaos* **6**, 867–887. (doi:10.1142/S0218127496000485)
- DiFrancesco, D. & Noble, D. 1985 A model of cardiac electrical activity incorporating ionic pumps and concentration changes. *Phil. Trans. R. Soc. B* **307**, 353–398.
- Doedel, E. J. & Kernévez, J. P. 1986 AUTO: software for continuation and bifurcation problems in ordinary differential equations with applications. Technical report, Applied Mathematics, California Institute of Technology.
- Ermentrout, B. 2002 *Simulating, analyzing, and animating dynamical systems: a guide to XPPAUT for researchers and students*. Philadelphia, PA: SIAM.
- Fink, M., Giles, W. R. & Noble, D. 2006 Contributions of inwardly rectifying  $K^+$  currents to repolarization assessed using mathematical models of human ventricular myocytes. *Phil. Trans. R. Soc. A* **364**, 1207–1222. (doi:10.1098/rsta.2006.1765)
- FitzHugh, R. A. 1961 Impulses and physiological states in theoretical models of nerve membrane. *Biophys. J.* **1**, 445–466.
- Fozzard, H. A. & Schoenberg, M. 1972 Strength–duration curves in cardiac Purkinje fibres: effects of liminal length and charge distribution. *J. Physiol.* **226**, 593–618.
- Garfield, R. E., Ali, M., Yallampalli, C. & Izumi, H. 1995 Role of gap junctions and nitric oxide in control of myometrial contractility. *Semin. Perinatol.* **19**, 41–51.
- Gheorghiadé, M., Adams, K. F. & Colucci, W. F. 2004 Digoxin in the management of cardiovascular disorders. *Circulation* **109**, 2959–2964. (doi:10.1161/01.CIR.0000132482.95686.87)
- Gima, K. & Rudy, Y. 2002 Ionic current basis of electrocardiographic waveforms: a model study. *Circ. Res.* **90**, 889–896. (doi:10.1161/01.RES.0000016960.61087.86)
- Harrison, S. M., McCall, E. & Boyett, M. R. 1992 The relationship between contraction and intracellular sodium in rat and guinea-pig ventricular myocytes. *J. Physiol.* **449**, 517–550.
- Hodgkin, A. L. & Huxley, A. F. 1952 A quantitative description of membrane current and its application to conduction and excitation in nerve. *J. Physiol.* **117**, 500–544.
- Holden, A. V. & Yoda, M. 1981 Ionic channel density of excitable membranes can act as a bifurcation parameter. *Biol. Cybern.* **42**, 29–38. (doi:10.1007/BF00335156)
- Joyner, R. W., Wang, Y., Wilders, R., Golod, D. A., Wagner, M. B., Kumar, R. & Goolsby, W. N. 2000 A spontaneously active focus drives a model atrial sheet more easily than a model ventricular sheet. *Am. J. Physiol.* **279**, H752–H763.
- Kass, R. S., Tsien, R. W. & Weingart, R. 1978 Ionic basis of transient inward current induced by strophanthidin in cardiac Purkinje fibres. *J. Physiol.* **281**, 209–226.
- Kleber, A. G. & Rudy, Y. 2004 Basic mechanisms of cardiac impulse propagation and associated arrhythmias. *Physiol. Rev.* **84**, 431–488. (doi:10.1152/physrev.00025.2003)
- Lindemans, F. W. & Vandergon, J. J. D. 1978 Current thresholds and liminal size in excitation of heart-muscle. *Cardiovasc. Res.* **12**, 477–485.
- Luo, C. H. & Rudy, Y. 1994 A dynamic model of the cardiac ventricular action potential. I. Simulations of ionic currents and concentration changes. *Circ. Res.* **74**, 1071–1096.
- Miake, J., Marban, E. & Nuss, H. B. 2002 Biological pacemaker created by gene transfer. *Nature* **419**, 132–133. (doi:10.1038/419132b)
- Miake, J., Marban, E. & Nuss, H. B. 2003 Functional role of inward rectifier current in heart probed by Kir2.1 over expression and dominant-negative suppression. *J. Clin. Invest.* **111**, 1529–1536. (doi:10.1172/JCI200317959)
- Nagumo, J., Animoto, S. & Yoshizawa, S. 1962 An active pulse transmission line simulating nerve axon. *Proc. Inst. Radio Engrs* **50**, 2061–2070.
- Silva, J. & Rudy, Y. 2003 Mechanism of pacemaking in  $I_{K1}$ -downregulated myocytes. *Circ. Res.* **92**, 261–263. (doi:10.1161/01.RES.0000057996.20414.C6)
- ten Tusscher, K. H. W. J., Noble, D., Noble, P. J. & Panfilov, A. V. 2004 A model for human ventricular tissue. *Am. J. Physiol.* **286**, H1573–H1589.

- Tong, W. C. & Holden, A. V. 2005 Induced pacemaker activity in virtual mammalian ventricular cells. *Lect. Notes Comput. Sci.* **3504**, 226–235.
- Tristani-Firouzi, M. *et al.* 2002 Functional and clinical characterization of KCNJ2 mutations associated with LQT7 (Andersen syndrome). *J. Clin. Invest.* **110**, 381–388. (doi:10.1172/JCI200215183)
- Varghese, A. & Winslow, R. L. 1993 Dynamics of the calcium subsystem in cardiac Purkinje fibers. *Physica* **68D**, 364–386.
- Varghese, A. & Winslow, R. L. 1994 Dynamics of abnormal pacemaking activity in cardiac Purkinje fibers. *J. Theor. Biol.* **168**, 407–420. (doi:10.1006/jtbi.1994.1121)
- Wilders, R., Wagner, M. B., Golod, D. A., Kumar, R., Wang, Y., Goolsby, W. N., Joyner, R. W. & Jongsma, H. J. 2000 Effects of anisotropy on the development of cardiac arrhythmias associated with focal activity. *Pflügers Arch.* **441**, 301–312. (doi:10.1007/s004240000413)
- Winslow, R. L., Varghese, A., Noble, D., Adlakha, C. & Hoythya, A. 1993 Generation and propagation of ectopic beats induced by spatially localized Na–K pump inhibition in atrial network models. *Proc. R. Soc. B* **254**, 55–61.
- Wray, S. 1993 Uterine contraction and physiological mechanisms of modulation. *Am. J. Physiol.* **264**, C1–C18.
- Yan, G. X., Shimizu, W. & Antzelevitch, C. 1998 Characteristics and distribution of M cells in arterially perfused canine left ventricular wedge preparations. *Circulation* **98**, 1921–1927.
- Zhang, H., Holden, A. V., Kodama, I., Honjo, H., Lei, M., Varghese, T. & Boyett, M. R. 2000 Mathematical models of action potentials in the periphery and center of the rabbit sinoatrial node. *Am. J. Physiol.* **279**, H397–H421.